




Design of the PI–UPFC–POD and PSS Damping Controllers Using an Artificial Bee Colony Algorithm

Luís Fabiano Barone Martins¹  · Percival Bueno de Araujo² · Elenilson de Vargas Fortes³  · Leonardo H. Macedo² 

Received: 2 April 2017 / Revised: 30 June 2017 / Accepted: 6 September 2017 / Published online: 19 September 2017
© Brazilian Society for Automatics–SBA 2017

Abstract This paper presents two variations of the artificial bee colony (ABC) algorithm, the classical and a modified version, called GBest, for the design of the proportional–integral and supplementary damping controllers: power system stabilizers and the unified power flow controller (UPFC)–power oscillation damping set. The objective is to insert additional damping to the low-frequency oscillation modes present in multimachine electrical power systems, to guarantee the small-signal stability of the system considering different loading conditions. A new current injection formulation for the UPFC is proposed and incorporated into the current sensitivity model used to represent the dynamical operation of the electric power system. Static and dynamical analysis were performed for the New England system to validate the proposed formulation and to evaluate the performance of the optimization algorithms. The results indicate that the modi-

fied version of the ABC algorithm has superior performance for this problem, providing robust solutions, that ensure the stability of the system even when small variations of the load are considered.

Keywords Artificial bee colony algorithm · Current sensitivity model · Power oscillation damping · Power system stabilizers · Unified power flow controller

1 Introduction

With the growing demand for electric energy, electrical power systems are increasingly subjected to high-load conditions, resulting in undesirable voltage levels and deviations in the operating frequency. These facts, together with the interconnections among various systems by means of long transmission lines and the action of automatic voltage regulators (AVRs) with high gains and low time constants, facilitate the appearance of low-frequency electromechanical oscillations, capable of harming the stability and the operation of the system (Anderson and Fouad 2003). The electromechanical oscillation modes are classified according to their frequency of occurrence, being the local (0.7–2.0 Hz) and inter-area (0.1–0.8 Hz) types the ones of more interest (Kundur 1994). For the safe operation of the system, it is essential that these modes are sufficiently damped. The small-signal stability study considered in this work assumes small variations in the system loading conditions and covers the analysis of the mentioned oscillation modes.

To overcome the negative effects on the stability of electrical power systems caused by the operation of the AVRs, a supplementary controller, called power system stabilizer (PSS), is included in the excitation system of the synchronous machines. The objective of the PSS is to insert electrical

✉ Luís Fabiano Barone Martins
luis.martins@ifpr.edu.br

Percival Bueno de Araujo
percival@dee.feis.unesp.br

Elenilson de Vargas Fortes
elenilson.fortes@ifg.edu.br

Leonardo H. Macedo
leohfmp@ieee.org

¹ Paraná Federal Institute of Education, Science, and Technology, Avenida Doutor Tito, s/n, Jacarezinho, PR 86400-000, Brazil

² São Paulo State University, Avenida Brasil Sul, 56, Centro, Ilha Solteira, SP 15385-000, Brazil

³ Goiás Federal Institute of Education, Science, and Technology, Rua Maria Vieira Cunha, 775, Residencial Flamboyant, Jataí, GO 75804-714, Brazil

torque in phase with the variations of the angular speed of the rotor (damping torque) (Demello and Concordia 1969; Larsen and Swann 1981). When adjusted, the PSS has great influence on local oscillation modes. However, in some cases, the PSS may not introduce the necessary damping to the inter-area modes (Cai and Erlich 2005). In view of this, flexible AC transmission systems (FACTS) are an interesting alternative, because in addition to improve the operation of the power system (Hingorani and Gyugyi 2000), they can insert additional damping to the inter-area oscillation modes when operating together with a power oscillation damping (POD) controller (Fortes et al. 2016a; Furini and Araujo 2008; Martins et al. 2016).

Among the existing FACTS devices, the unified power flow controller (UPFC), the focus of this work, is one of the most complete, because of its ability to manage (simultaneously or not) the active and reactive power flows in the transmission line in which its series converter is installed and the voltage magnitude at the bus where its shunt converter is connected (Gyugyi et al. 1995).

The correct parameterization of the supplementary controllers is fundamental for damping the low-frequency oscillations to guarantee the stability of the power system. Several approaches have been successfully used to achieve this goal, including the residue method (Yang et al. 1998), the Nyquist stability criterion (Zhenenko and Farah 1984), and the decentralized modal control (DMC) method (Furini et al. 2011; Valle and Araujo 2015). The coordinated and simultaneous tuning of these controllers is a complex optimization problem with multiple local minima. Thus, in addition to the approaches focused on classical control theory, other studies were carried out using different optimization techniques to obtain adequate adjustments.

Among these techniques, the stochastic bio-inspired ones, such as those based on the genetic algorithms (GAs) (Fortes et al. 2016b; Hassan et al. 2014), particle swarm optimization (PSO) (Menezes et al. 2016; Shayeghi et al. 2010), and the artificial bee colony algorithm (ABC) (Abedinia et al. 2011; Martins et al. 2016), can be cited. All the search approaches used by the cited works are inspired by behaviors observed in nature. The GA and the PSO are based on evolutionary biology (Goldberg 1989) and on the dynamics of the flight of birds (Kennedy and Eberhart 1995), respectively. In the case of the ABC, the inspiration comes from the foraging behavior of honeybee swarms (Karaboga 2005). Alternatively, meta-heuristic optimization techniques that extend local search frameworks to avoid local optimal solutions, but are not bio-inspired, such as the variable neighborhood search (Fortes et al. 2018), were also used to solve this problem.

This work investigates the effects of the UPFC FACTS device in combination with the supplementary damping controllers (PSSs and POD) to the small-signal stability of power systems. To do so, the power system is represented by a lin-

ear model called current sensitivity model (CSM), based on Kirchhoff’s current law (Fortes et al. 2016b; Pádua Júnior et al. 2013). Because of this, a linear model for the UPFC, based on current injection, is proposed. The currents are calculated by an expanded power flow formulation based on the mismatches of the current injection equations on each bus of the system, differently from the proposal presented in Kopcak et al. (2007), where nodal power injections are used. The control system used in the UPFC model consists of proportional–integral (PI) controllers, similar to that presented Valle and Araujo (2015), but coupled to the shunt voltage source converter (VSC).

In this work, the design of supplementary damping controllers (PI–UPFC–POD and PSSs) is formulated as an optimization problem and the classical and GBest (Global Best) ABC algorithms are used to solve it. The problem is formulated to optimize two objective functions, based on the eigenvalues of the electrical power system, comprising the minimum damping factor and the difference between the natural undamped frequencies of the desired and calculated eigenvalues of interest, considering three operating points for the system. The controllers are tuned with the optimization of these functions, guaranteeing the stability of the system for the desired operating region. The performances of the proposed algorithms are evaluated using the New England multimachine system under different loading conditions.

From the above, the main contributions of this study are: (i) to present a current injection model for the UPFC; (ii) to develop and use an expanded power flow tool based on mismatches currents in the polar form to determine the UPFC injections; (iii) to implement the classical and GBest versions of the ABC algorithm; and (iv) to compare their performances with respect to the coordinated tuning of the parameters of the supplementary damping controllers (PSSs and UPFC–POD) and the PI controllers of the UPFC.

2 Power System Modeling

2.1 Expanded Power Flow

The mismatch of the injected current at bus k ($\Delta \hat{I}_k$) is determined using the balance of the specified current phasor (\hat{I}_k^{spe}) and the calculated current phasor (\hat{I}_k^{calc}), as illustrated in Fig. 1 and shown in (1).

$$\Delta \hat{I}_k = \hat{I}_k^{\text{spe}} - \hat{I}_k^{\text{calc}} = \hat{I}_{Gk} - \hat{I}_{Lk} - \sum_{m \in \Omega_k} \hat{I}_{km} = 0 \quad (1)$$

The variables \hat{I}_{Gk} , \hat{I}_{Lk} , and \hat{I}_{km} , that appear in (1), are the phasors of the injected and demanded current at bus k , and the current through branch km , respectively. The set Ω_k represents all buses connected to bus k .

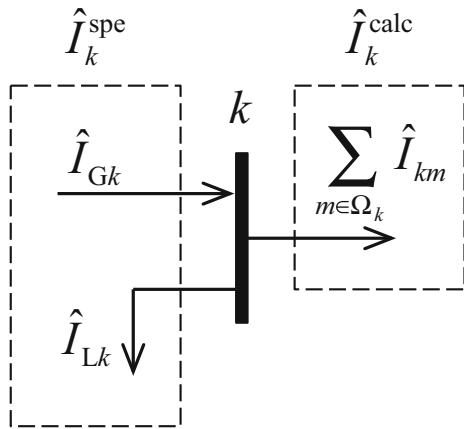


Fig. 1 Current balance at bus k

Rewriting (1) as a function of the active (P_k^{spe}) and reactive (Q_k^{spe}) specified powers of the conventional power flow, the voltage phasor at bus k ($V_k \angle \theta_k$), the conductance (G_{km}), and susceptance (B_{km}) of branch km , and separating the resulting current in real (ΔI_{rk}) and imaginary (ΔI_{ik}) parts, the components of the mismatches of the currents at bus k , shown in (2) and (3), are obtained.

$$\Delta I_{rk} = \frac{(P_k^{spe} \cos \theta_k + Q_k^{spe} \sin \theta_k)}{V_k} - \sum_{m \in \kappa} V_m (G_{km} \cos \theta_m - B_{km} \sin \theta_m) \tag{2}$$

$$\Delta I_{ik} = \frac{(P_k^{spe} \sin \theta_k - Q_k^{spe} \cos \theta_k)}{V_k} - \sum_{m \in \kappa} V_m (G_{km} \sin \theta_m + B_{km} \cos \theta_m) \tag{3}$$

In (2) and (3), the set κ is formed by the union of the set Ω_k and bus k . By applying the Newton–Raphson (NR) method to (2) and (3), the matrix formulation (4), that represents the linearized system used to determine the algebraic variables of the power flow, is obtained.

$$\begin{bmatrix} \Delta I_r \\ \Delta I_i \end{bmatrix} = \begin{bmatrix} \frac{\partial \Delta I_r}{\partial \theta} & \frac{\partial \Delta I_r}{\partial V} \\ \frac{\partial \Delta I_i}{\partial \theta} & \frac{\partial \Delta I_i}{\partial V} \end{bmatrix} \begin{bmatrix} \Delta \theta \\ \Delta V \end{bmatrix} \tag{4}$$

2.2 Current Mismatches Equations

The mismatches of the current components ΔI_{rk} and ΔI_{ik} at bus k can be expressed as function of the mismatches of the active (ΔP_k) and reactive (ΔQ_k) powers, of the conventional

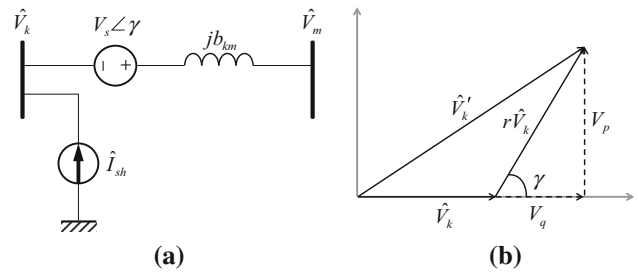


Fig. 2 a Equivalent circuit, b phasor diagram of the UPFC

formulation of the power flow problem, as shown in (5).

$$\begin{aligned} \Delta I_{rk} &= \frac{\Delta P_k \cos \theta_k + \Delta Q_k \sin \theta_k}{V_k} = 0 \\ \Delta I_{ik} &= \frac{\Delta P_k \sin \theta_k - \Delta Q_k \cos \theta_k}{V_k} = 0 \end{aligned} \tag{5}$$

2.3 Current Injection Model for the UPFC

The UPFC controller can be represented by two VSC converters, one in series with the transmission line (VSC1) and the other in shunt at the installation bus (VSC2). The connection of the UPFC to the power system is performed by coupling transformers (Noroozian et al. 1997). Due to the use of these converters, the UPFC is able to perform simultaneous (or not) control of the voltage magnitude at the connection bus of the VSC2 and the power flow on the transmission line of VSC1.

In the UPFC equivalent circuit shown in Fig. 2a, the transmission line is represented by its susceptance ($j b_{km}$), the converter VSC1 is represented by a synchronous voltage source, while the converter VSC2 is represented by an ideal current source. Based on the current injection equations for the UPFC obtained from Meng and So (2000), the approach presented in Huang et al. (2000) is applied, where the voltage phasor \hat{V}_s is decomposed in terms of its in phase (V_q) and quadrature (V_p) components, as illustrated in Fig. 2b. Thus, (6)–(10), that determine the real and imaginary components of the current injections carried out by the device installed between buses k and m , are obtained.

$$C1 = \frac{V_m}{V_k} (V_p \cos \theta_{km} + V_q \sin \theta_{km}) b_{km} \tag{6}$$

$$I_{rk}^{upfc} = C1 \cos \theta_k + (V_q b_{km} + I_q) \sin \theta_k \tag{7}$$

$$I_{ik}^{upfc} = C1 \sin \theta_k - (V_q b_{km} + I_q) \cos \theta_k \tag{8}$$

$$I_{rm}^{upfc} = -(V_p \cos \theta_k + V_q \sin \theta_k) b_{km} \tag{9}$$

$$I_{im}^{upfc} = -(V_p \sin \theta_k - V_q \cos \theta_k) b_{km} \tag{10}$$

The current injection model for the UPFC is shown in Fig. 3. This representation is appropriate for both small-signal stability studies and static analysis.

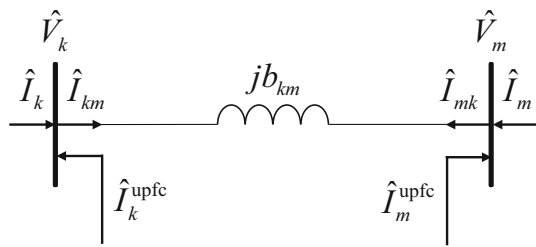


Fig. 3 Current injection model for the UPFC

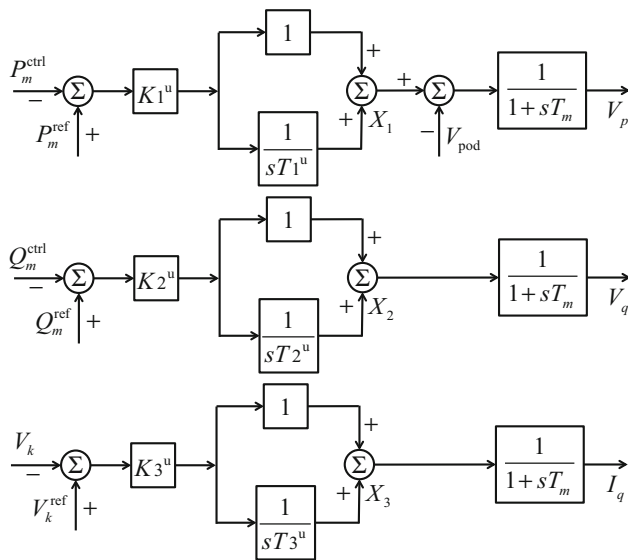


Fig. 4 Structure of the control system of the UPFC

2.4 Configuration of the Control System of the UPFC

In order to perform the control of the power flows by the UPFC in the common buses of its installation, PI controllers are used (Fortes et al. 2016b; Valle and Araujo 2015) (see Fig. 4).

From Fig. 4, it can be seen that the PI controllers are responsible for modulating the control variables (V_p , V_q , and I_p) of the converters VSC1 and VSC2. In this structure, the parameters of the controllers are represented by the gains $K1^u$, $K2^u$, and $K3^u$ (in p.u.) and by the time constants $T1^u$, $T2^u$, and $T3^u$ (in seconds). In addition, the time constant T_m is the inherent delay of the control device and is in the range of 1–10 ms (Hingorani and Gyugyi 2000). The supplementary signal of the POD controller is V_{pod} and, in this work, is used to modulate the quadrature component (V_p) of the converter VSC1.

In Fig. 4, the specified values of the active and reactive power flows in line km and the voltage magnitude at bus k are P_m^{ref} , Q_m^{ref} , and V_k^{ref} , respectively.

The complex power ($\hat{S}_m^{ctrl} = P_m^{ctrl} + j Q_m^{ctrl}$) controlled by the UPFC can be obtained by performing the nodal power balance at bus m of the system, as shown in (11).

$$\hat{S}_m^{ctrl} = \hat{S}_m^{upfc} - \hat{S}_{mk} \tag{11}$$

In (11), \hat{S}_m^{upfc} and \hat{S}_{mk} represent, in this order, the complex power injected by the FACTS at bus m and the complex power flow from bus m to bus k . By separating (11) into real and imaginary parts, the active (P_m^{ctrl}) and reactive (Q_m^{ctrl}) power flows controlled by the UPFC are obtained.

2.5 Inclusion of the UPFC Equations in the Power Flow Modeled by Current Injections

In order to observe the operation of the UPFC in the power system, it is necessary that its equations are added to the power flow. For this purpose, it is assumed that its state variables are constant with respect to time, which makes their temporal derivatives equal to zero. This consideration makes the differential equations of the UPFC become algebraic equations. In this way, the problem is restricted to the determination of the zeros of a set of nonlinear algebraic equations, whose solution can be obtained using the NR algorithm in the same way as in a conventional power flow (Kopcak et al. 2007). Since, in this work, the power flow modeling was performed by current injection, the essence of the problem is to satisfy all current mismatches at the installation buses of the UPFC k and m , as shown in (12) and (13).

$$\Delta \hat{I}_k = \hat{I}_k^{esp} - \hat{I}_k^{calc} + \hat{I}_k^{upfc} = 0 \tag{12}$$

$$\Delta \hat{I}_m = \hat{I}_m^{esp} - \hat{I}_m^{calc} + \hat{I}_m^{upfc} = 0 \tag{13}$$

In (12) and (13), \hat{I}_k^{upfc} and \hat{I}_m^{upfc} are the phasors of current injections at the UPFC installation buses k and m , due to the converters VSC1 and VSC2. It is important to note that in the other buses of the system, the mismatches of the current components do not differ from the power flow equations presented.

By linearizing the system formed by the equations resulting from the substitution in (12) and (13) of the current injections of the UPFC and of the current mismatches defined in (6)–(10) and (2)–(3), respectively, and by the set of dynamical equations ($\dot{x}_u = f_u(x_u, y)$), obtained from Fig. 4, the matrix formulation of the expanded power flow by current injection (14) is obtained.

In (14), $\Delta x_u = [\Delta V_p \ \Delta X1 \ \Delta V_q \ \Delta X2 \ \Delta I_q \ \Delta X3]^T$ are the linearized state variables of the PI controllers of the UPFC and the matrix $J4_u$ is defined in (15).

$$\begin{bmatrix} J_{1u} \\ \frac{\partial f_u}{\partial x_u} \\ \vdots \\ \frac{\partial f_{rk}}{\partial x_u} \\ \vdots \\ \frac{\partial f_{rm}}{\partial x_u} \\ \vdots \\ \frac{\partial f_{ik}}{\partial x_u} \\ \vdots \\ \frac{\partial f_{im}}{\partial x_u} \\ \vdots \\ \frac{\partial f_{nb}}{\partial x_u} \\ J_{2u} \end{bmatrix} = \begin{bmatrix} \overbrace{0 \cdots \frac{\partial f_u}{\partial \theta_k} \cdots \frac{\partial f_u}{\partial \theta_m} \cdots 0}^{J_{1u}} & \overbrace{0 \cdots \frac{\partial f_u}{\partial V_k} \cdots \frac{\partial f_u}{\partial V_m} \cdots 0}^{J_{2u}} \\ \vdots & \vdots \\ J4_{pf}^{11} + J4_u^{11} & J4_{pf}^{12} + J4_u^{12} \\ \vdots & \vdots \\ 0 & 0 \\ \vdots & \vdots \\ J4_{pf}^{21} + J4_u^{21} & J4_{pf}^{22} + J4_u^{22} \\ \vdots & \vdots \\ 0 & 0 \\ \vdots & \vdots \\ 0 & 0 \\ J_{2u} \end{bmatrix} \begin{bmatrix} \Delta x_u \\ \Delta \theta_1 \\ \vdots \\ \Delta \theta_k \\ \vdots \\ \Delta \theta_m \\ \Delta \theta_{nb} \\ \Delta V_1 \\ \vdots \\ \Delta V_k \\ \vdots \\ \Delta V_m \\ \Delta V_{nb} \end{bmatrix} \tag{14}$$

$$J4_u = \begin{bmatrix} 0 \cdots 0 \cdots 0 \cdots 0 & \vdots & \vdots & \vdots & \vdots \\ \vdots & \vdots & \vdots & \vdots & \vdots \\ 0 \cdots \frac{\partial I_{rk}^{upfc}}{\partial \theta_k} \cdots \frac{\partial I_{rk}^{upfc}}{\partial \theta_m} \cdots 0 & \cdots & 0 \cdots \frac{\partial I_{rk}^{upfc}}{\partial V_k} \cdots \frac{\partial I_{rk}^{upfc}}{\partial V_m} \cdots 0 \\ \vdots & \vdots & \vdots & \vdots & \vdots \\ 0 \cdots \frac{\partial I_{rm}^{upfc}}{\partial \theta_k} \cdots \frac{\partial I_{rm}^{upfc}}{\partial \theta_m} \cdots 0 & \cdots & 0 \cdots \frac{\partial I_{rm}^{upfc}}{\partial V_k} \cdots \frac{\partial I_{rm}^{upfc}}{\partial V_m} \cdots 0 \\ \vdots & \vdots & \vdots & \vdots & \vdots \\ 0 \cdots 0 \cdots 0 \cdots 0 & \cdots & 0 \cdots 0 \cdots 0 \cdots 0 \\ \vdots & \vdots & \vdots & \vdots & \vdots \\ 0 \cdots \frac{\partial I_{ik}^{upfc}}{\partial \theta_k} \cdots \frac{\partial I_{ik}^{upfc}}{\partial \theta_m} \cdots 0 & \cdots & 0 \cdots \frac{\partial I_{ik}^{upfc}}{\partial V_k} \cdots \frac{\partial I_{ik}^{upfc}}{\partial V_m} \cdots 0 \\ \vdots & \vdots & \vdots & \vdots & \vdots \\ 0 \cdots \frac{\partial I_{im}^{upfc}}{\partial \theta_k} \cdots \frac{\partial I_{im}^{upfc}}{\partial \theta_m} \cdots 0 & \cdots & 0 \cdots \frac{\partial I_{im}^{upfc}}{\partial V_k} \cdots \frac{\partial I_{im}^{upfc}}{\partial V_m} \cdots 0 \\ \vdots & \vdots & \vdots & \vdots & \vdots \\ 0 \cdots 0 \cdots 0 \cdots 0 & \cdots & 0 \cdots 0 \cdots 0 \cdots 0 \end{bmatrix} \tag{15}$$

2.6 Dynamical Models for the PSS and POD Controllers

In this work, the structures used to represent the supplementary damping controllers (PSS and POD) differ only by the input and output signals. The basic structure is shown in Fig. 5.

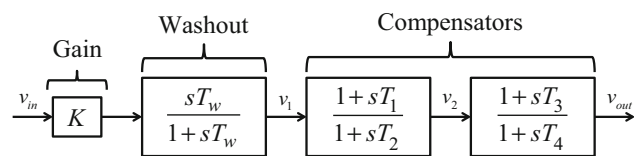


Fig. 5 Basic structure of the PSS and POD controllers

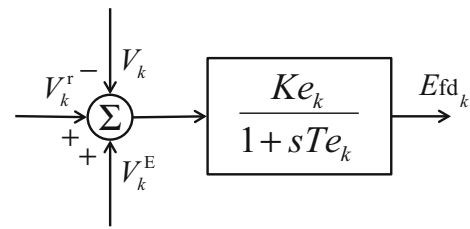


Fig. 6 Automatic voltage regulator model

This structure consists of a gain K that determines the amount of damping introduced by the controllers, a washout block that functions as a high-pass filter with a time constant T_w conveniently adjusted to allow the controller to operate only during transient periods, and a phase compensation block (usually $T_1 = T_3$ and $T_2 = T_4$) that provides the appropriate phase advance characteristics to compensate for the phase delay between the control loop output of the AVR and the torque produced by the generator (Kundur 1994).

For the PSSs, the input signal, v_{in} , is the angular speed (ω_k) of the rotor of the generator k , whereas for the POD, the input is the active power flow (P_{km}) of the transmission line adjacent to the installation of the UPFC–POD set. The intermediate signals v_1 and v_2 for the PSSs are: V_1k and V_2k and, for the POD: Y_1 and Y_2 . The output signals, v_{out} , for the PSSs are the voltage V_k^E added to the AVR control loop shown in Fig. 6, together with the bus voltage (V_k) and its voltage reference (V_k^r). For the POD, v_{out} assumes the value of the voltage V_{pod} , that will be included in the control loop of the VSC1, according to Fig. 4.

2.7 Current Sensitivity Model

The power system is represented by a linear model called current sensitivity model (CSM), based on the Kirchoff’s current law, that must be satisfied even when the system suffers a small-signal perturbation (Fortes et al. 2016b; Pádua Júnior et al. 2013). An important feature of this tool is that it maintains all the system buses in the model, which facilitates the inclusion of FACTS-POD and PSSs devices.

In the CSM, the dynamics of a multimachine electrical power system consisting of ng generators, nb buses, np PSSs, and an UPFC–POD set is described according to Eqs. (16)–(19).

$$\Delta x_T = \begin{bmatrix} [\Delta \omega_1 \cdots \Delta \omega_{ng}] [\Delta \delta_1 \cdots \Delta \delta_{ng}] [\Delta E'_{q1} \cdots \Delta E'_{qng}] \\ [\Delta Efd_1 \cdots \Delta Efd_{ng}] [\Delta V_{11} \cdots \Delta V_{1np}] [\Delta V_{21} \cdots \Delta V_{2np}] \\ [\Delta V_1^{pss} \cdots \Delta V_{np}^{pss}] \Delta x_u^t [\Delta Y_1 \Delta Y_2 \Delta V_{sup}]^t \end{bmatrix} \tag{16}$$

$$\Delta u_T = \begin{bmatrix} [[\Delta P_1^m \cdots \Delta P_{ng}^m] [\Delta V_1^r \cdots \Delta V_{ng}^r] [\Delta P_{L1} \cdots \Delta P_{Lng}] \\ [\Delta Q_{L1} \cdots \Delta Q_{Lng}] \Delta P_m^{ref} \Delta P_m^{ref} \Delta Q_m^{ref} \Delta Q_m^{ref} \Delta V_k^{ref} \Delta V_k^{ref}]^t \end{bmatrix} \tag{17}$$

$$\Delta y = [[\Delta \theta_1 \cdots \Delta \theta_{nb}] [\Delta V_1 \cdots \Delta V_{nb}]]^t \tag{18}$$

$$\begin{bmatrix} \Delta \dot{x}_T \\ \mathbf{0} \end{bmatrix} = \begin{bmatrix} \mathbf{J1}_T & \mathbf{J2}_T \\ \mathbf{J3}_T & \underbrace{\mathbf{J4}_{pf} + \mathbf{J4}_u}_{\mathbf{J4}_T} \end{bmatrix} \cdot \begin{bmatrix} \Delta x_T \\ \Delta y \end{bmatrix} + \begin{bmatrix} \mathbf{B1}_T \\ \mathbf{B2}_u \end{bmatrix} \cdot [\Delta u_T] \quad (19)$$

In (19), the submatrices $\mathbf{J1}_T$, $\mathbf{J2}_T$, $\mathbf{J3}_T$, and $\mathbf{J4}_T$ associate the state variables of the complete system (angular speed ($\Delta\omega$), internal angle of the rotor ($\Delta\delta$), internal quadrature ($\Delta E'_q$) and field (ΔE_{fd}) voltages of the generator, control parameters of the converters VSC1 and VSC2 of the UPFC (ΔV_p , ΔV_q , and ΔI_p) and auxiliary variables (ΔX_1 , ΔX_2 , and ΔX_3), variables of the PSSs (ΔV_{1k} , ΔV_{2k} , and ΔV_k^E), and variables of the POD (ΔY_1 , ΔY_2 , and ΔV_{pod}) with the algebraic variables (voltage magnitude (ΔV) and angle ($\Delta\theta$) at the buses of the power system). The input variables are the mechanical power (ΔP^m), the reference voltage of the AVR (ΔV^r), the active (ΔP_L) and reactive (ΔQ_L) loads, the active (ΔP_m^{ref}) and reactive (ΔQ_m^{ref}) power references, and the voltage reference (ΔV_k^{ref}) of the PI controllers of the UPFC, related to submatrices $\mathbf{B1}_T$ and $\mathbf{B2}_u$.

The space state representation is obtained by eliminating Δy of the system defined in (19), which results in the state matrix $\mathbf{A} = \mathbf{J1}_T - \mathbf{J2}_T \mathbf{J4}_T^{-1} \mathbf{J3}_T$ and input matrix $\mathbf{B} = \mathbf{B1}_T - \mathbf{J2}_T \mathbf{J4}_T^{-1} \mathbf{B2}_u$.

Algorithm 1: Artificial Bee Colony Algorithm

- 1: Initialize the population of solutions z_i using (20) and evaluate it;
 - 2: cycle \leftarrow 1;
 - 3: Repeat;
 - 4: Create the new solutions v_i for the employed bees with (21) and evaluate it;
 - 5: Apply the greedy selection process for the employed bees;
 - 6: Calculate p_i for z_i using (22);
 - 7: Create v_i for the onlookers from z_i selected according to p_i and evaluate it;
 - 8: Apply the greedy selection process for the onlookers;
 - 9: Determine the abandoned solution for the scout bee, if it exists, and replace it with a new solution z_i randomly generated;
 - 10: Store the best solution achieved so far;
 - 11: cycle \leftarrow cycle + 1;
 - 12: Until cycle = MCN.
-

3 Techniques for the Design of the Supplementary Damping Controllers

3.1 Artificial Bee Colony Algorithm

The ABC algorithm is based on the collective behavior of a swarm of bees in the search for food and has been successfully applied in several optimization problems (Karaboga and Akay 2009). Although there are several types of tasks in a real beehive, the ABC algorithm uses a simplified model that mimics the search for sources of food, that are equivalent to the solutions of the problem, by employed bees, onlookers, and scouts (Karaboga et al. 2007).

Half of the colony is formed by employed bees, and the other half is formed by onlookers. Employed bees store the neighborhood information from their food sources and pass it on to onlooker bees that tend to select the best sources. Then, they intensify the search around the selected food source. The scout bees are formed by some employed bees, who abandon their food sources and randomly search for other sources. These steps are repeated up to a maximum number of iterations it_{max} or until a stop criterion is satisfied.

The ABC algorithm has some advantages in relation to other bio-inspired algorithms such as GAs and the PSO, among them the good balance between the intensification and diversification processes (Akay and Karaboga 2012) and the need for a smaller number of control parameters (Karaboga and Akay 2009).

The initial population of candidate solutions is formed by SN sources of food, randomly generated. A food source $z_i = [z_{i1} \ z_{i2} \dots \ z_{id}]$ is a d -dimensional vector, where d is the number of variables in the optimization problem. The initial population is obtained through (20).

$$z_{ij} = z_{ij}^{min} + \varepsilon_{ij} (z_{ij}^{max} - z_{ij}^{min}) \quad (20)$$

In (20) $i = \{1, 2, \dots, SN\}$, $j = \{1, 2, \dots, d\}$, z_{ij}^{min} and z_{ij}^{max} are, respectively, the upper and lower bound of each variable and ε_{ij} is a random number in the interval $[0, 1]$. Each one of the SN sources of food will be occupied by an employed bee, and the value of the evaluation function $F(z_i)$ will be calculated.

After the initialization, the population is evaluated, and then, each employed bee, placed in z_i , generates a new food source, v_i , in the neighborhood of its current position using (21).

$$v_{ij} = z_{ij} + \phi_{ij} (z_{ij} - z_{kj}) \quad (21)$$

In (21), $k \in \{1, 2, \dots, SN\}$ and $j \in \{1, 2, \dots, d\}$ are randomly chosen indexes, with k different from i , and ϕ_{ij} is a random number in the interval $[-1, 1]$.

Once v_i is determined, it will be evaluated and compared to z_i . If the evaluation function of v_i is better than or equal to z_i , then v_i will replace z_i in the population; otherwise, z_i will be maintained. In other words, a greedy selection mechanism, between the old and new candidate solution, is employed.

After the employed bees complete their searches, they share information about the amount of nectar (objective function value) of their best food sources with the observing bees in the hive dance area. An onlooker bee evaluates this information for all employed bees and selects a food source based on a probability p_i related to the amount of nectar. This probabilistic selection depends on the values of the evaluation function obtained from the current set of solutions. In the

classical ABC, the roulette wheel selection mechanism, in which each slice has the size proportional to the value of the evaluation function, is used, as shown in (22).

$$p_i = \text{fit}_i / \sum_{n=1}^{BN} \text{fit}_n \quad (22)$$

In (22), fit_i is the value of the evaluation function of solution i . Thus, the greater fit_i is, the greater the probability that the i th food source is selected, considering a maximization problem.

Once the onlooker bee selects its source of food z_i , it modifies it using (21). As in the case of employed bees, if this modified source v_i has an amount of nectar greater than or equal to the amount of z_i , this new source will replace z_i and will become a new member of the population.

If a source of food z_i cannot be improved after a limit of lmt attempts, it must be abandoned and the employed bee in charge of exploring it becomes a scout bee. It will randomly search for a new source of food, as shown in (20).

It is possible to identify from the above that the ABC algorithm has three control parameters: the number of sources of food SN , which is equal to the number of employed and onlooker bees, the limit value lmt , and the maximum number of iterations it_{max} . The detailed pseudocode of the ABC algorithm is shown in Algorithm 1.

3.2 Artificial Bee Colony Algorithm Global Best

The ABC GBest algorithm seeks to improve the capacity to intensify the local search of the classical ABC algorithm. For this, (21) is replaced by (23), as proposed by (Gao et al. 2012).

$$v_{ij} = z_{best\ j} + \phi_{ij} (z_{r1\ j} - z_{r2\ j}) \quad (23)$$

In (23), $z_{best\ j}$ is the best solution, j , of the population and the indices $r1$ and $r2$ are mutually exclusive integers chosen randomly within the set $\{1, 2, \dots, N\}$ and different from index i . With this modification, we intend to overcome two problems of the classical algorithm: the first one is related to the rate of convergence of the solution for unimodal problems, usually smaller than the rate of other population-based algorithms such as the PSO algorithm. The second problem is the ease with which the classical algorithm gets stuck in

local optimal solutions when it involves complex multimodal problems (Karaboga and Akay 2009).

4 Problem Formulation

For an electrical power system to operate safely in terms of small-signal stability, it is necessary that the damping coefficients (ξ) of its low-frequency oscillation modes assume sufficiently positive values, even with possible loading changes.

In this sense, this work proposes a new objective function $F(z)$ that should be able to lead the search of the optimization algorithm within the space of solutions for determining a tuning for the parameters of the controllers that guarantee enough damping for the system even with variations in its operating point. For this purpose, three loading levels are considered: nominal ($P^{spc} + jQ^{spc}$) and $\pm 10\%$ of nominal variation. It is expected to ensure the highest possible damping for any operating point within the specified loading range. In addition, $F(z)$ should ensure that the frequencies of the oscillation modes of interest, ω^{calc} , obtained at the end of the parameterization process, do not suffer too much alteration in relation to those frequencies obtained without the operation of the controllers. Thus, for each iteration of ABC algorithm, the eigenvalues of interest must be selected and directed to the left semi-plane of the complex plane.

From the above considerations, at each iteration, the damping matrix $\xi \in \mathbb{R}^{q \times p}$ and the distances matrix $\delta \in \mathbb{R}^{n \times p}$, with each element $\delta_{ij} = |\omega_{ij}^{des} - \omega_{ij}^{calc}|$, will be defined. The dimensions p , q , and n represent, in this order, the number of operating points considered for the system, the number of damping coefficients of each solution, and the number of eigenvalues of interest. These matrices, together with the dimensionless constant η (defined empirically), will be used as input values for the evaluation of $F(z)$, defined in (24).

$$F(z) = \eta |1 - \min(\xi)| + \sum_{j=1}^p \sum_{i=1}^n \delta_{ij} \quad (24)$$

In the proposed method, for a system with ng generators, np PSSs, and an UPFC–POD set, both ABC algorithms will provide a set of gains and time constants for each PSS, for the POD, and for the PI controllers of the UPFC, as a solution. In this way, the solution is represented by a vector consisting of the parameters of ns supplementary damping controllers, according to (25).

$$z_i = \left[\underbrace{T_1^u \ K_1^u \ T_3^u \ K_3^u}_{UPFC} \ \underbrace{T_1^{pod} \ T_2^{pod} \ K^{pod}}_{POD} \ \underbrace{T_{11}^{pss} \ T_{21}^{pss} \ K_1^{pss}}_{PSS1} \ \dots \ \underbrace{T_{1np}^{pss} \ T_{2np}^{pss} \ K_{np}^{pss}}_{PSSnp} \right] \quad (25)$$

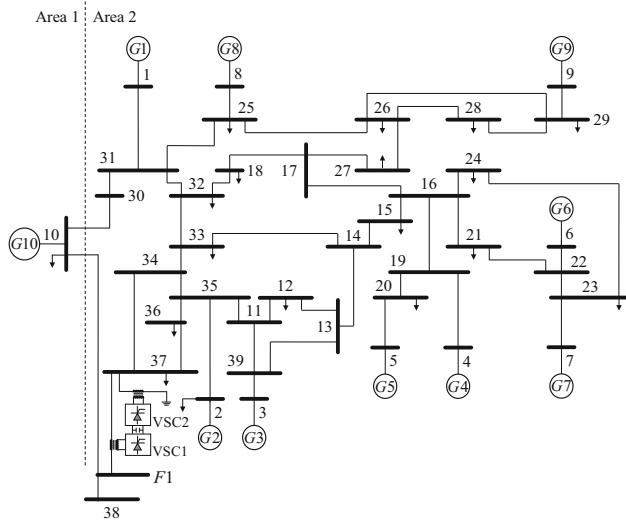


Fig. 7 One-line diagram of the New England system

5 Tests and Results

5.1 Steady-State Analysis of the Power System

The tests were conducted using the New England system, whose data can be found in (Fortes et al. 2016b). Its one-line diagram, with the inclusion of the UPFC-POD set, is shown in Fig. 7. For the installation of this device, it was necessary to create a fictitious branch, $F_1 - 37$, consisting of the coupling reactance of the transformer that connects the VSC1, which was assumed to be 0.01 p.u. The choice of the FACTS installation site, between buses 37 and 38, has two justifications: to improve the voltage profiles at buses 12, 15, 33, 34, 36, and 37, that are below the $\pm 5\%$ interval limit, and to introduce damping to the inter-area mode.

When the UPFC is not operating in the system performing its functions of voltage and power flow control (situation that will be referred to as the base case), the variables related to the VSCs are zero, indicating the inexistence of power injections by the device. In this operating condition, the power flow in the line $F_1 - 38$ is $-16.41 - j121.50$ MVA and the voltage magnitude at bus 37 is 0.94 p.u.

To adjust the voltage magnitudes within the acceptable range of $\pm 5\%$, the power flow in the line $F_1 - 38$ and the voltage magnitude at bus 37, controlled by the UPFC, were adjusted to $-75 - j150$ MVA and 1.0 p.u., respectively. The voltage profiles of the system before (base case) and after the actuation of the UPFC are shown in Fig. 8.

By analyzing Fig. 8, it can be verified that the voltage problems were corrected. In this operating condition, the UPFC control variables assume the values (in p.u.) of $V_p = -0.101$, $V_q = -0.094$, and $I_q = 2.882$.

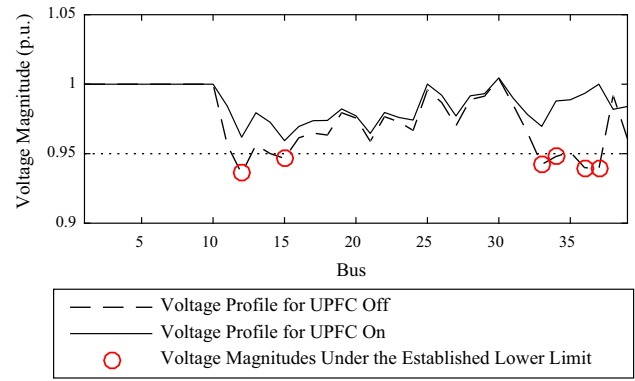


Fig. 8 System’s voltage profile for the specified loading with and without the actuation of the UPFC

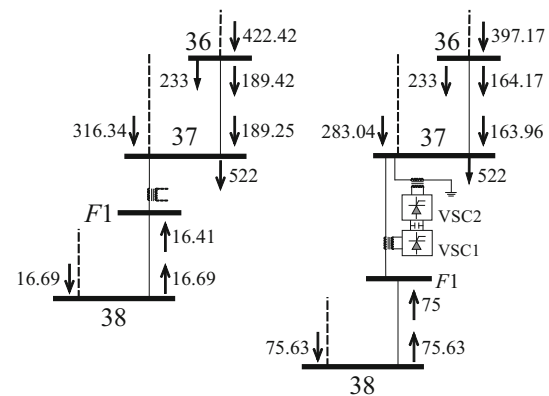


Fig. 9 Active power control performed by the UPFC

The active power flows (MW) near the fictitious bus, for the two cases analyzed, are shown in Fig. 9.

The comparison between the power flows before and after the operation of the UPFC allows us to verify that it does not provide active power to the system, since all the active power generated (consumed) by the VSC1 is consumed (generated) by the VSC2. In this way, the device re-manages the active flows in order to implement the specified control. With the data presented in Fig. 9, it is possible to perform the nodal active power balance (in MW) for the installation buses of the UPFC and, thus, to validate the power flow control performed by the device.

For the base case (UPFC not operating), the eigenvalues of interest (λ_i) of the state matrix of the power system are presented in Table 1, as well as the associated oscillation frequencies (ω_{ni}) and damping coefficients (ξ_i).

The eigenvalues shown in Table 1 indicate that the system presents, in this point of operation, eight local oscillation modes, three of them unstable (L1–L3) and five weakly damped modes (L4–L8). In addition, there is a weakly damped inter-area mode (I1). This characterizes the oscillation instability of the system for this operating condition.

Table 1 Dominant eigenvalues, natural undamped frequencies, and damping coefficients for the base case

Mode	Eigenvalue	ω_{ni} (Hz)	ξ (p.u.)
L1	$0.1717 \pm j5.9098$	0.9410	-0.0290
L2	$0.1291 \pm j6.3571$	1.0120	-0.0203
L3	$0.0848 \pm j6.8490$	1.0901	-0.0124
I1	$-0.0015 \pm j3.4821$	0.5542	0.0004
L4	$-0.1068 \pm j6.4583$	1.0280	0.0165
L5	$-0.1982 \pm j8.2615$	1.3152	0.0240
L6	$-0.2516 \pm j8.3149$	1.3240	0.0302
L7	$-0.2114 \pm j7.1701$	1.1417	0.0295
L8	$-0.2703 \pm j8.0966$	1.2893	0.0334

To increase the damping of the oscillation modes in the system to the highest possible levels, eight PSSs (one for each local mode) will be installed at generators G1–G5 and G7–G9, according to the participation factors criterion presented in (Kundur 1994). Also, a UPFC–POD set, responsible for damping the inter-area mode, will be installed between buses 37 and 38. The local input signal adopted for the POD is the active power variation (ΔP_{km}) through line 37–34.

5.2 Performance of the Methods

For the definition of the supplementary damping controller settings, three operating points (90, 100 and 110% of the nominal loading) will be evaluated. The values assigned to the parameters of the ABC algorithm are: SN = 20; lmt = 320 (lmt = $0.5 \times \text{SN} \times D_{\max}$, where D_{\max} is the dimension of the problem, in this case $D_{\max} = 32$), and $it_{\max} = 500$.

For both ABC algorithms, the bounds for the time constants (seconds) and gains (p.u.) for the POD were: $0.01 \leq T1^{\text{pod}} \leq 0.25$, $0.25 \leq T2^{\text{pod}} \leq 0.5$, and $0.1 \leq K^{\text{pod}} \leq 0.5$; for the UPFC: $0.001 \leq T1^u \leq 0.1$, $0.01 \leq T3^u \leq 1$, $0.001 \leq K1^u \leq 0.5$, and $1 \leq K3^u \leq 10$; and for the PSSs: $0.5 \leq T1_k^{\text{pss}} \leq 1.5$, $0.01 \leq T2_k^{\text{pss}} \leq 0.5$, and $1 \leq K_k^{\text{pss}} \leq 15$. The time constant T_m was assumed to be 0.001 s.

To evaluate the performance of the algorithms, two cases were considered for the FACTS device in the power system: (I) assuming the PI–UPFC–POD set operating and (II)

assuming the PI–UPFC–POD set not operating. In both cases, eight PSSs were installed at generators G1–G5 and G7–G9. In addition, 25 trials were performed for each version of the algorithm for the two cases, using the objective function defined in (24). The data presented in Table 2 provide a general statistical overview of the results determined by each algorithm after 2500 iterations for each case.

By examining Table 2, it can be seen that the solutions obtained by the two versions of the ABC algorithm in Case I produce results for the minimum damping better than those provided by the algorithms in Case II, demonstrating the role of the PI–UPFC–POD for improving the damping of the oscillations in the system. In addition, considering Case I as being of interest (thanks to the better results), it is observed by analyzing the statistical metrics, the superiority of the GBest version of the algorithm over the classical one, for both cases.

Figure 10 shows the mean evolution, along the iterations, of the minimum damping in the system obtained with the tuning provided by the algorithms for Case I. Its examination reinforces the superiority of the ABC GBest algorithm over the classical one, since the GBest provided solutions that lead the system to operate with higher damping levels, on average.

Since the ABC GBest algorithm achieved superior performance for all established criteria and for both cases, the parameters obtained by it will be used for the adjustment of the controllers in the results in the following section.

5.3 Small-Signal Stability Analysis

The set of parameters used to tune the controllers was the one obtained in the test that presented the highest minimum damping value after 2500 iterations of the algorithm, considering Case I. Tables 3 and 4 show the values of the parameters of the PSSs, UPFC–POD, and PI provided by the ABC GBest algorithm.

For the nominal loading level and after the parameterization of the supplementary controllers, it can be seen from Table 5 that the previously unstable system (see Table 1) begins to operate with the damping of the eigenvalues within the specified range. The region in the complex plane of the eigenvalues of interest for the base case and for Case I (Fig. 11) reinforces this conclusion.

Table 2 Comparison of the performance of the algorithms for 25 tests

Case	Method	Damping coefficients (p.u.)				
		Best	Worst	Mean	Median	SD
I	ABC	0.1563	0.0685	0.1136	0.1128	0.0200
	ABC GBest	0.1623	0.1092	0.1307	0.1282	0.0137
II	ABC	0.1040	0.0664	0.0861	0.0854	0.0112
	ABC GBest	0.1111	0.0704	0.0946	0.0930	0.0111

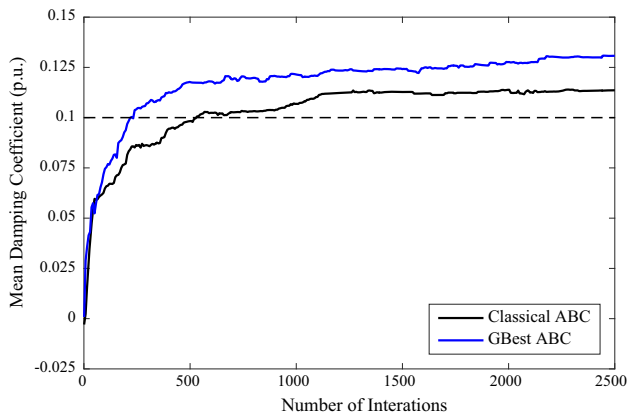


Fig. 10 Evolution of the damping coefficients for Case I

Table 3 Gains and time constants of the PSS and POD controllers adjusted by the ABC GBest

Device	T_1 (s)	T_2 (s)	K (p.u.)
PSS 1	1.5000	0.0505	15.000
PSS 2	1.0637	0.1197	11.327
PSS 3	0.8084	0.1184	10.658
PSS 4	0.7402	0.1039	6.5083
PSS 5	0.7238	0.1976	8.7635
PSS 7	0.9496	0.1721	0.6787
PSS 8	0.8733	0.0928	15.000
PSS 9	0.5113	0.1852	5.7099
POD	0.1333	0.4189	0.2368

Table 4 Gains and time constants of the PI controllers adjusted by the ABC GBest

$T_1 = T_2$ (s)	T_3 (s)	$K_1 = K_2$ (p.u.)	K_3 (p.u.)	T_m (s)
0.0277	0.0522	9.2951	0.0101	0.001

The high margin of stability to small perturbations provided by the solution can be observed when the mechanical power of the generator 1 undergoes a disturbance (step) of 0.05 p.u.

In order to verify the minimum damping of the system (with the controllers parameterized according to Tables 3 and 4), under operating conditions different from those considered in the optimization process of the ABC GBest algorithm, but within the range evaluated (90% to 110% of the load for the base case), five operating points were considered, as shown in Fig. 12.

By analyzing Fig. 12, it is possible to conclude that the value of the minimum damping in the system remains above 15%, when the variation of the load is considered. Regarding the maximum damping of the eigenvalues of interest, there is a visible variation in the range, which is reasonable, given the fact that there is no control over these values. In this way, the

Table 5 Dominant eigenvalues, natural undamped frequencies, and damping coefficients for the solution

Mode	Eigenvalue	ω_{ni} (Hz)	ξ (p.u.)
L1	$-2.1797 \pm j4.4624$	0.7904	0.4389
L2	$-2.0544 \pm j4.9836$	0.8579	0.3811
L3	$-1.3863 \pm j6.4093$	1.0437	0.2114
I1	$-1.2817 \pm j3.0712$	0.5296	0.3851
L4	$-3.3638 \pm j5.1354$	0.9770	0.5479
L5	$-3.3483 \pm j7.7447$	1.3429	0.3968
L6	$-2.2253 \pm j8.5425$	1.4050	0.2521
L7	$-3.1197 \pm j6.4484$	1.1401	0.4355
L8	$-1.5271 \pm j8.0026$	1.2966	0.1874

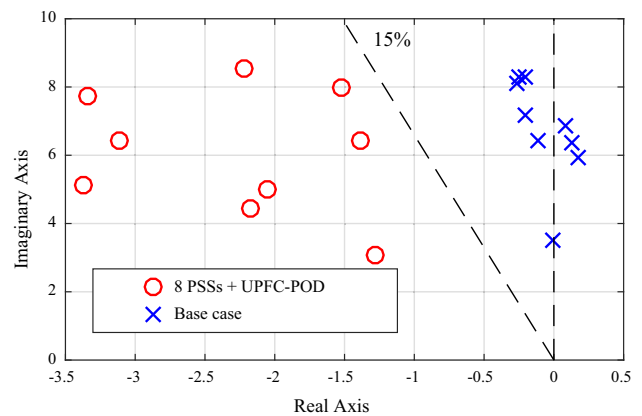


Fig. 11 Eigenvalues positions

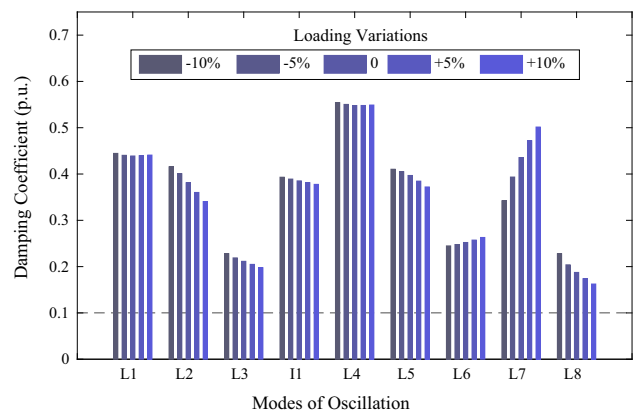


Fig. 12 Damping of the oscillation modes considering the loading variations

New England system operates with a high level of damping in all cases studied, showing the robustness of the solution obtained by ABC GBest algorithm.

6 Conclusion

This work presented two variants of the artificial bee colony (ABC) algorithm—the classical version and the ABC GBest—applied to the problem of the design of the proportional–integral (PI) and supplementary damping controllers: power system stabilizers (PSSs) and the unified power flow controller (UPFC)—power oscillation damping (POD) set. The main objective was to determine a robust coordinated tuning for the parameters of these controllers that inserted the desired damping to the multimachine electrical power system.

It was also proposed a new model for the UPFC based on current injections, for both static and dynamical analysis. The static analysis performed using the New England system validated the model presented for the UPFC. In relation to the dynamical analysis, it was possible to conclude that the ABC GBest algorithm was more efficient than the classical ABC algorithm for the design of the controllers. The results indicated that the system remained stable, with high damping margin, even in different loading scenarios, demonstrating the robustness of the parameterization obtained.

Acknowledgements This work was supported by the Paraná Federal Institute of Education, Science, and Technology (IFPR), Coordination for the Improvement of Higher Education Personnel (CAPES), and the São Paulo Research Foundation (FAPESP), under Grant 2016/10992-9.

References

- Abedinia, O., Wyns, B., & Ghasemi, A. (2011). Robust fuzzy PSS design using ABC. In *2011 10th International Conference on Environment and Electrical Engineering (EEEIC)*. doi:10.1109/EEEIC.2011.5874849.
- Akay, B., & Karaboga, D. (2012). Artificial bee colony algorithm for large-scale problems and engineering design optimization. *Journal of Intelligent Manufacturing*, 23(4), 1001–1014. doi:10.1007/s10845-010-0393-4.
- Anderson, P. M., & Fouad, A. A. (2003). *Power system control and stability* (2nd ed.). Piscataway, NJ: Wiley-IEEE Press.
- Cai, L.-J., & Erlich, I. (2005). Simultaneous coordinated tuning of PSS and FACTS damping controllers in large power systems. *IEEE Transactions on Power Systems*, 20(1), 294–300. doi:10.1109/TPWRS.2004.841177.
- Demello, F. P., & Concordia, C. (1969). Concepts of synchronous machine stability as affected by excitation control. *IEEE Transactions on Power Apparatus and Systems, PAS*, 88(4), 316–329. doi:10.1109/TPAS.1969.292452.
- Fortes, E. V., Araujo, P. B., Macedo, L. H., Gamino, B. R., & Martins, L. F. B. (2016a). Analysis of the influence of PSS and IPFC-POD controllers in small-signal stability using a Simulated Annealing algorithm. In *2016 12th IEEE International Conference on Industry Applications (INDUSCON)*. doi:10.1109/INDUSCON.2016.7874512.
- Fortes, E. V., Araujo, P. B., & Macedo, L. H. (2016). Coordinated tuning of the parameters of PI, PSS and POD controllers using a Specialized Chu-Beasley's Genetic Algorithm. *Electric Power Systems Research*, 140, 708–721. doi:10.1016/j.epr.2016.04.019.
- Fortes, E. V., Macedo, L. H., Araujo, P. B., & Romero, R. (2018). A VNS algorithm for the design of supplementary damping controllers for small-signal stability analysis. *International Journal of Electrical Power & Energy Systems*, 94, 41–56. doi:10.1016/j.ijepes.2017.06.017.
- Furini, M. A., & Araujo, P. B. (2008). Melhora da estabilidade dinâmica de sistemas elétricos de potência multimáquinas usando o dispositivo FACTS “thyristor-controlled series capacitor—TCSC”. *SBA: Controle & Automação Sociedade Brasileira de Automática*, 19(2), 214–225.
- Furini, M. A., Pereira, A. L. S., & Araujo, P. B. (2011). Pole placement by coordinated tuning of power system stabilizers and FACTS-POD stabilizers. *International Journal of Electrical Power & Energy Systems*, 33(3), 615–622. doi:10.1016/j.ijepes.2010.12.019.
- Gao, W., Liu, S., & Huang, L. (2012). A global best artificial bee colony algorithm for global optimization. *Journal of Computational and Applied Mathematics*, 236(11), 2741–2753. doi:10.1016/j.cam.2012.01.013.
- Goldberg, D. E. (1989). *Genetic algorithms in search, optimization, and machine learning* (1st ed.). Boston, MA: Addison-Wesley.
- Gyugyi, L., Schauder, C. D., Williams, S. L., Rietman, T. R., Torgerson, D. R., & Edris, A. (1995). The unified power flow controller: A new approach to power transmission control. *IEEE Transactions on Power Delivery*, 10(2), 1085–1097. doi:10.1109/61.400878.
- Hassan, L. H., Moghavvemi, M., Almurib, H. A. F., & Muttaqi, K. M. (2014). A coordinated design of PSSs and UPFC-based stabilizer using genetic algorithm. *IEEE Transactions on Industry Applications*, 50(5), 2957–2966. doi:10.1109/TIA.2014.2305797.
- Hingorani, N. G., & Gyugyi, L. (2000). *Understanding FACTS: Concepts and technology of flexible AC transmission systems* (1st ed.). New York, NY: Wiley-IEEE Press.
- Huang, Z., Ni, Y., Shen, C. M., Wu, F. F., Chen, S., & Zhang, B. (2000). Application of unified power flow controller in interconnected power systems-modeling, interface, control strategy, and case study. *IEEE Transactions on Power Systems*, 15(2), 817–824. doi:10.1109/59.867179.
- Karaboga, D. (2005). An idea based on honey bee swarm for numerical optimization. *Technical Report-TR06*, Erciyes University.
- Karaboga, D., & Basturk, B. (2007). Artificial bee colony (ABC) optimization algorithm for solving constrained optimization problems. In P. Melin, O. Castillo, L. T. Aguilar, J. Kacprzyk, & W. Pedrycz (Eds.), *Foundations of fuzzy logic and soft computing. Lecture notes in computer science* (Vol. 4529). Berlin: Springer. doi:10.1007/978-3-540-72950-1_77.
- Karaboga, D., & Akay, B. (2009). A comparative study of artificial bee colony algorithm. *Applied Mathematics and Computation*, 214(1), 108–132. doi:10.1016/j.amc.2009.03.090.
- Kennedy, J., & Eberhart, R. (1995). Particle swarm optimization. *1995 IEEE International Conference on Neural Networks (ICNN)*. doi:10.1109/ICNN.1995.488968.
- Kopcak, I., Costa, V. F., & Silva, L. C. P. (2007). A generalized load flow method including the steady state characteristic of dynamic devices. In *2007 IEEE Lausanne Power Tech*. doi:10.1109/PCT.2007.4538297.
- Kundur, P. (1994). *Power system stability and control* (1st ed.). New York, NY: McGraw-Hill Education.
- Larsen, E. V., & Swann, D. A. (1981). Applying power system stabilizers part II: Performance objectives and tuning concepts. *IEEE Transactions on Power Apparatus and Systems, PAS*, 100(6), 3025–3033. doi:10.1109/TPAS.1981.316410.
- Martins, L. F. B., Gamino, B. R., Araujo, P. B., Fortes, E. V., & Miotto, E. L. (2016). Comparison between artificial bee colony and particle swarm optimization algorithms in the tuning of PSS and UPFC-POD controllers. In *2016 12th IEEE International Conference on*

- Industry Applications (INDUSCON)*. doi:[10.1109/INDUSCON.2016.7874534](https://doi.org/10.1109/INDUSCON.2016.7874534).
- Menezes, M. M., Araujo, P. B., & Valle, D. B. (2016). Design of PSS and TCSC damping controller using particle swarm optimization. *Journal of Control, Automation and Electrical Systems*, 27(5), 554–561. doi:[10.1007/s40313-016-0257-z](https://doi.org/10.1007/s40313-016-0257-z).
- Meng, Z. J., & So, P. L. (2000). A current injection UPFC model for enhancing power system dynamic performance. In *2000 IEEE Power Engineering Society Winter Meeting*. doi:[10.1109/PESW.2000.850212](https://doi.org/10.1109/PESW.2000.850212).
- Noroozian, M., Angquist, L., Ghandhari, M., & Andersson, G. (1997). Use of UPFC for optimal power flow control. *IEEE Transactions on Power Delivery*, 12(4), 1629–1634. doi:[10.1109/61.634183](https://doi.org/10.1109/61.634183).
- Pádua Júnior, C. R., Takahashi, A. L. M., Furini, M. A., & Araujo, P. B. (2013). Proposta de um modelo para análise de estabilidade a pequenas perturbações baseado na lei de Kirchhoff para correntes. In *2013 XI Simpósio Brasileiro de Automação Inteligente (SBAI)*.
- Shayeghi, H., Safari, A., & Shayanfar, H. A. (2010). PSS and TCSC damping controller coordinated design using PSO in multi-machine power system. *Energy Conversion and Management*, 51(12), 2930–2937. doi:[10.1016/j.enconman.2010.06.034](https://doi.org/10.1016/j.enconman.2010.06.034).
- Valle, D. B., & Araujo, P. B. (2015). The influence of GUPFC FACTS device on small signal stability of the electrical power systems. *International Journal of Electrical Power & Energy Systems*, 65, 299–306. doi:[10.1016/j.ijepes.2014.10.012](https://doi.org/10.1016/j.ijepes.2014.10.012).
- Yang, N., Liu, Q., & McCalley, J. D. (1998). TCSC controller design for damping interarea oscillations. *IEEE Transactions on Power Systems*, 13(4), 1304–1310. doi:[10.1109/59.736269](https://doi.org/10.1109/59.736269).
- Zhenenko, G. N., & Farah, H. B. (1984). Simultaneous optimization of the adjustable parameters in multimachine power systems. *Electric Power Systems Research*, 7(2), 103–108. doi:[10.1016/0378-7796\(84\)90019-1](https://doi.org/10.1016/0378-7796(84)90019-1).